SAE INTERNATIONAL

Aluminum Extrusions for Automotive Crash Applications

2017-01-1272

Published 03/28/2017

Nick Parson
RTA

Jerome Fourmann
Rio Tinto Alcan

Jean-Francois Beland
National Research Council Canada

CITATION: Parson, N., Fourmann, J., and Beland, J., "Aluminum Extrusions for Automotive Crash Applications," SAE Technical Paper 2017-01-1272, 2017, doi:10.4271/2017-01-1272.

Abstract

One of the main applications for aluminum extrusions in the automotive sector is crash structures including crash rails, crash cans, bumpers and structural body components. The objective is usually to optimize the energy absorption capability for a given structure weight. The ability to extrude thin wall multi-void extrusions contributes to this goal. However, the alloy used also plays a significant role in terms of the ability to produce the required geometry, strength - which to a large extent controls the energy absorption capability and the “ductility” or fracture behavior which controls the strain that can be applied locally during crush deformation before cracking. This paper describes results of a test program to examine the crush behavior of a range of alloys typically supplied for automotive applications as a function of processing parameters including artificial ageing and quench rate.

Introduction

The use of Al-Mg-Si aluminum extrusions for automotive crash management systems has grown significantly in the last 10 years due to the superior specific energy absorption capabilities as compared to steel. This is in part related to the ability of 6xxx alloys to be extruded into complex multi-cavity profiles which generate multiple plastic hinges contributing to the overall energy absorption. In terms of performance requirements the crash structure has to absorb the required energy level without exceeding a maximum load. Associated material specifications for axial crush structures typically involve a yield strength requirement along with some measure of cracking tendency such as CXX[1] where XX is the YS/10 in MPa with a certain degree of cracking allowed. The grading of cracking is somewhat subjective and is naturally dependent on the material and the profile geometry and thickness. A grading from 0 to 20 is widely used in Europe where a crash index of 0 represents complete fragmentation and 20 is assigned to zero cracking. Much of the literature[2, 3] related to material selection and alloy design for crush applications generally deals with fracture in crush in this qualitative manner. Minor cracks are probably not an issue but at some point, cracking will start to adversely affect the energy absorption behavior. However, the stage at which this occurs is not clear and as current numerical simulations typically use the tensile stress strain curve to characterize the material behavior, they do not have the capability to predict material fracture accurately. Many automotive specifications use elongation in a tensile test as a measure of the ability to resist fracture. The current work explores the usefulness of this parameter as compared to alternatives such as true fracture strain. In terms of energy absorption, typically the undulating force displacement curve associated with the sequential fold formation is averaged[4] to give a mean crush force (MCF). Generally this aspect is not dealt with in the materials development literature where it is assumed that higher strength automatically increases energy absorption. The current work explores how this parameter is linked to the results of a standard tensile test.

There is a general trend to provide higher strength solutions for crash systems, for example C28 or C32 which can allow down-gauging. In addition to weight saving, reducing wall thickness also has some benefit in reducing the maximum strain imposed during crush. However, as the minimum wall thickness achievable in the extrusion process generally increases with stronger 6XXX alloys this may not always be achievable. In testing a range of 6xxx extruded materials in lateral crush Rubeuffet et al[5] found it very difficult to produce an intrinsic material classification and found that final material selection is very much dependent on the required energy absorption and geometry constraints specific to a given automotive application. Nevertheless it is clear that in order to develop improved extruded materials and integrate material behavior into numerical simulations, there is a need to develop reliable mechanical testing protocols and data that deal with energy absorption and fracture behavior in both axial and lateral crush.

The present paper extends the authors' earlier work[6,7] and deals with axial crush of a range of commonly used dilute and medium strength 6xxx extruded materials in a range of tempers. The work is part of a longer term joint program between Rio Tinto Aluminium and the Canadian National Research Council, to develop improved extrusion materials for automotive applications and to develop simulation tools for crush applications that accurately take account of material behavior including fracture. Compared to steel the strain rate sensitivity of aluminum at room temperature is low. Therefore, in order to compare a wide range of materials and conditions a simple "quasi-static" test protocol was adopted for the study.

Experimental

Nine 6XXX alloy compositions corresponding to commercial alloy variants within AA6060, AA6063, AA6008, AA6005A, AA6061 and AA6082 were DC cast as 101mm dia. billets and homogenized to standard commercial practices. General Purpose (GP) and High Strength (HS) versions of AA6060 and AA6063 were included. The former represented traditional compositions whereas the latter were typical of more recent compositions optimized in terms of the Mg/Si ratio. The Mg and Si contents are illustrated in Figure 1 along with the lines corresponding to Mg/Si atomic ratios of 1/1 and 2/1. AA6061 was close to the traditional 2/1 balanced Mg_2Si line and the AA6008, GP6060 and GP6063 had intermediate Mg/Si ratios. The remaining compositions were close to the 1/1 Mg/Si ratio. The AA6063 and AA6060 variants, along with the AA6008 had Mn additions <.10wt%. The latter also had a deliberate V addition of ~0.1wt%. The medium strength alloys contained various Mn and Cr additions; AA6005A ~ .3wt%Mn, AA6082 ~ 0.5wt%Mn, AA6061 ~ 0.1wt%Cr, AA6082Cr ~ 0.5wt%Mn and 0.1wt%Cr.

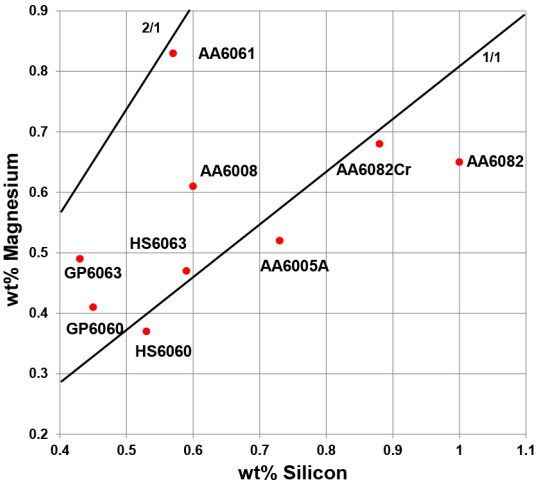

Figure 1. Mg and Si Contents of Test Materials.

The material was extruded on the Rio Tinto 780 tonne experimental press into a 40 x 30mm hollow profile with an extrusion ratio of 32:1, a wall thickness of 2mm and an external corner radius of 5mm. The profile had been previously established to be discriminating in terms of crush behavior for a range of strength levels[6]. The die was designed to position the extrusion welds in the middle of the flat faces away from the higher strain regions at the profile corners during crush testing. A billet temperature of 500°C was used and the speed was controlled to produce exit temperatures of at least 550°C to ensure good press solutionizing. It is well established[1,2,6] that quench rate after extrusion has an effect on crush ductility. The two AA6063 variants were processed using both forced air and a "water standing wave" quench units. All remaining alloy variants were only processed using water quenching. The time - temperature curve during quenching was measured using a clip-on high speed wireless logger and the resulting quench curves are shown in Figure 2. The water quench rate from 500-250°C was ~ 1000°C/s whereas the corresponding air quench was 4°C/sec. The 6XXX materials were aged to various times at temperatures of 150, 175, 200 and 215°C to produce a range of tempers including peak aged along with multiple underaged and overaged tempers, resulting in strength reductions of 10 - 50% of the peak yield strength. The full list of heat treatments is given in Table 1.

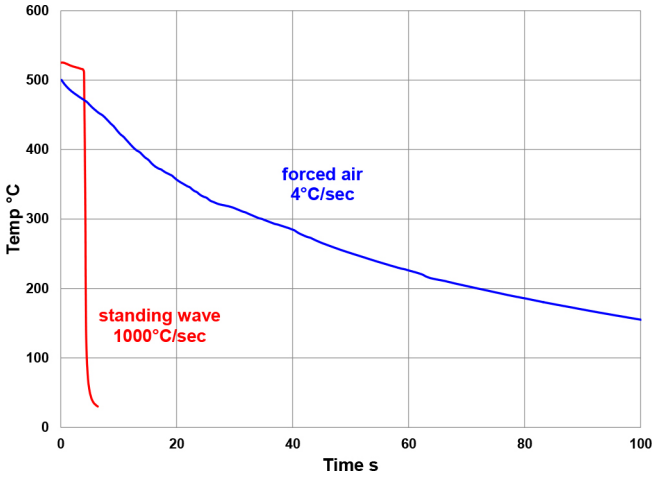

Figure 2. Water and air quench rates for 40 x 3mm Profile.

Table 1. Artificial Ageing Conditions.

	150°C				175°C					200°C			215°C				
Time hrs	5	8	12	16	2	3	5	8	16	2	3	8	2	2.5	5	7	8
GP6060																	
GP6063																	
HS6060																	
HS6063																	
AA6008																	
AA6005A																	
AA6061																	
AA6082																	
AA6082Cr																	

Crush testing was carried out using a 650kN Interlaken servo-press with a crosshead speed of 20mm/s. The bottom of each column was fixed in a recess while the top was unrestrained. The column length was reduced from 150 to 60mm during crushing. An elliptic paraboloid indentation was applied 19mm from the top of the column to provide consistent initiation. This had been previously shown to significantly reduce scatter in crush force measurements[6]. Force - displacement data was recorded. This was numerically integrated to produce an energy absorbed vs. distance relationship which was used to generate the mean crush force (MCF) - distance curve. To avoid

the effect of the initial peak load, the MCF value was averaged between crush distances of 40 and 80mm. The degree of cracking during crush was assessed qualitatively using a grading scale from 1 to 9, with a grade of 1 (zero cracking) being the best available and a grade of 9 representing complete disintegration. Figure 3 summarizes the crush rating system with typical images for each grade. It should be noted that grades 6 and 7 were used to discriminate between cracking on internal and external folds. During crush the external folds are restricted by the internal folds such that the latter experience a tighter bend radius[6].

Tensile testing was conducted for each alloy/temper combination according to ASTM E8 using a 50mm gauge length. The resulting fracture surfaces were imaged in a stereo microscope and an image analysis routine was developed and utilized to determine the area of the final fracture (A_f) on both sides of the failure. True fracture strain values (ε_f) were then calculated based on $\varepsilon_f = \ln(A_o/A_f)$ where A_o is the original cross section area and Af is the area at the final fracture.

The microstructures of the extrusions were assessed by standard optical metallography techniques.

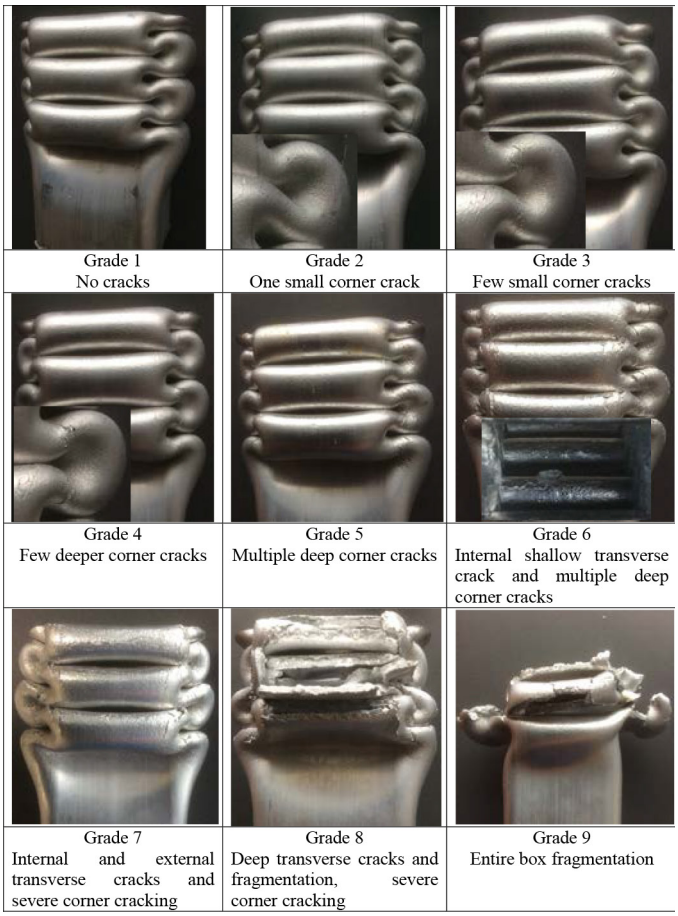

Figure 3. Crush grading system

Results

Soft 6XXX YS < 270MPa (GP6060, GP6063, HS6060, HS6063)

All four alloys were fully recrystallized to a fine mean grain size of <100µ as shown in Figure 4. This was associated with the low levels of dispersoid forming elements present in these types of dilute materials. The GP variants of 6060 and 6063 represent more traditional versions of these alloys, containing a slight excess of silicon calculated based on a Mg/Si atomic ratio of 2/1. The HS versions have Mg levels close to the lower limit of the respective AA specifications and the Si was calculated to be balanced based on a Mg/Si ratio of ~1. Combined with the artificial ageing variants (Table 1) this allowed a yield strength range of ~120-270 MPa and a UTS range of 180 to 280MPa to be covered. Figure 5 presents MCF values for each alloy and the temper variants as a function of yield and tensile strengths. The HS6060 and HS6063 variants exhibited minor grade 2 cracking in the peak aged condition (indicated by blue circles in Figure 5) but otherwise all the variants were crack free. The MCF/YS plot in Figure 5, gave a type of hysteresis behavior with temper. For each alloy the peak aged condition gave the highest crush force and this corresponded to the 16hrs/175°C ageing treatment. Moving in a clockwise direction, each series of points for a particular alloy represents the transition from underaged to peak aged to overaged such that for the same YS value an underaged condition could increase the MCF by ~ 4-8% compared to an overaged temper. For this reason YS is a poor predictor of energy absorption in crush due to the high strains involved and the MCF behavior with temper is mainly due to the effects of alloy and ageing treatment on the UTS. As shown in Figure 6, over a tensile strength range of ~ 180- 280MPa the MCF followed a linear relationship with UTS. The solid line and symbols represent the water quenched extrusions and the dashed line and open symbols correspond to air quench material. Again cracking is indicated by circles. With water quenching cracking was only minor (grade 2). In these cases, the results indicate that it is possible to delay cracking and increase MCF by switching from HS6060 to HS6063 or by adjustment of the temper. With air quenching, the UTS values for the two AA6063 variants was reduced, the severity of cracking increased to grade 4 and the occurrence of cracking was shifted to lower UTS values.

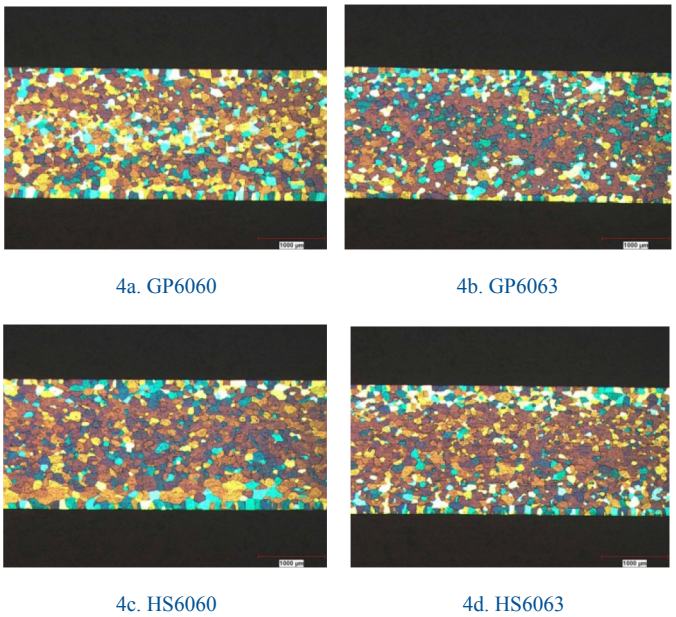

4a. GP6060 4b. GP6063

4c. HS6060 4d. HS6063

Figure 4. Grain Structures of Soft Alloy Variants. (longitudinal, Barkers reagent)

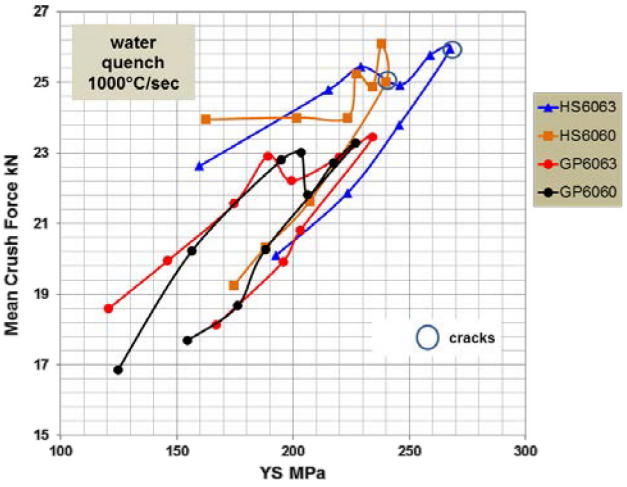

Figure 5. Mean crush force vs, YS - soft alloy variants

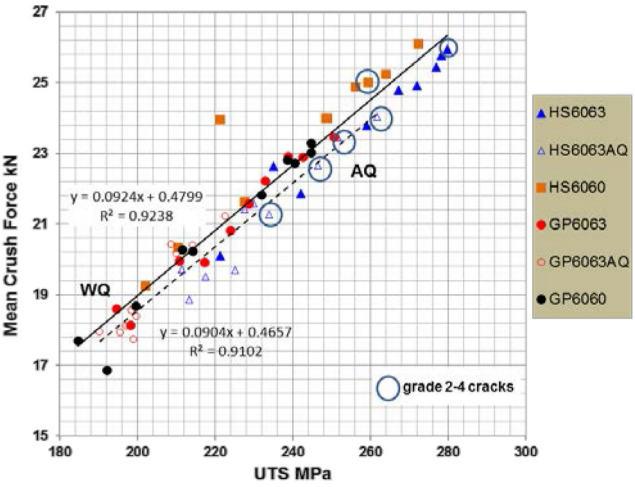

Figure 6. Mean crush force vs. UTS - soft alloy variants including air and water quench

In most cases the peak YS corresponded with the peak UTS except for the HS6060 where some of the under-aged (in terms of YS) tempers actually gave the highest UTS. Therefore specifying the material requirements for a crashbox application in terms of YS is not sufficient to define the energy absorption behavior.

Figure 7 compares the appearance of the crush samples of peak aged HS6063 for the air quenched and water quenched conditions. Although air quenching resulted in a lower strength material the severity of cracking was more severe with grade 4 corner cracks as compared to minor grade 2 cracking for the stronger water quenched material.

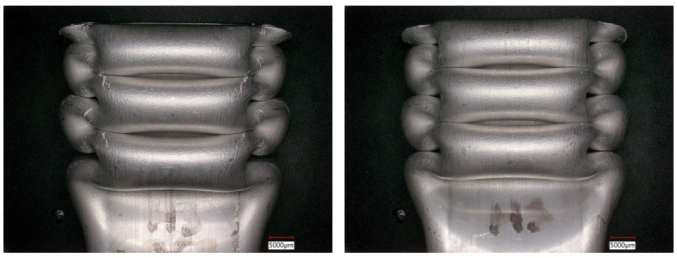

7a. Air quenched (260MPa) G2 7b. Water quenched (280MPa) G4

Figure 7. Effect of quench rate on cracking tendency in crush for HS6063. UTS values in parentheses.

It is useful to compare the cracking behavior for these soft 6XXX alloys with the measures of ductility that can be obtained from a longitudinal tensile test. Figure 8 presents the crush rating as a function of tensile elongation. All the data is for water quenched material except for the open symbols which represent air quenched HS6063. In the water quenched condition, the two materials that exhibited cracking (peak aged HS6063 and HS6060) were associated with a tensile elongation of ~ 11.5%, whereas materials that successfully crushed without any cracks had elongation values ranging from 8 - 19%. Cracking for the air quenched HS6063 was associated with elongation values of 11-16%, whereas material with a tensile elongation of 10% was crack free. These results demonstrate the unsuitability of this parameter as an indicator of crush behavior. In contrast the use of the true fracture strain, as shown in Figure 9, gave a clear cut off for cracking/no cracking conditions for the same materials and a near linear deterioration in the crush rating with decreasing fracture strain. Based on these results, the critical fracture strain for the profile tested in this study was ~ 0.7.

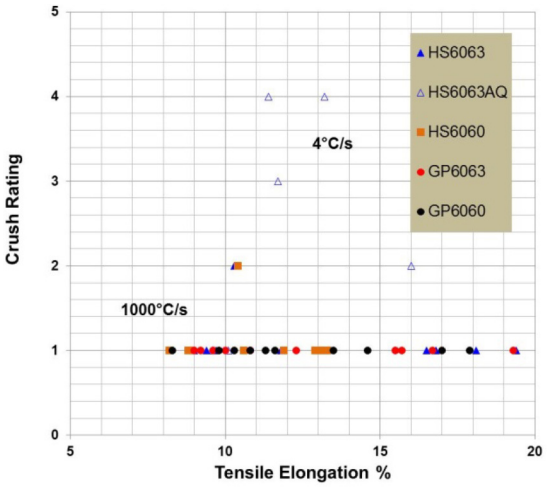

Figure 8. Crush rating vs. tensile elongation soft alloy variants including air and water quench

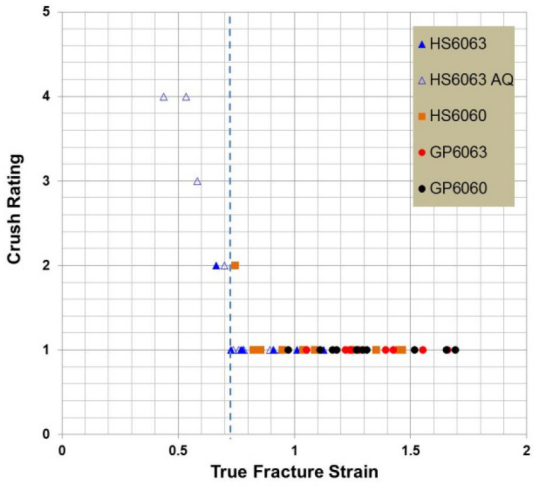

Figure 9. Crush rating vs. true fracture strain - soft alloy variants including air and water quench

Medium Strength Alloys YS > 270MPa (AA6008, AA6005A, AA6061, AA6082, AA6082Cr)

The extruded microstructures for the 5 medium strength alloys are shown in Figure 10. The sections were taken in the longitudinal direction at the ¼ width position on the 40mm face to avoid the weld lines. The AA6008 was fully recrystallised with a grain size of ~ 100µ, similar to the earlier soft alloys which is again due to the low dispersoid content of this alloy. It also contained a deliberate addition of 0.1wt%V and after etching, longitudinal banding was evident. This is associated with the segregated V solute distribution carried over from the cast ingot. Additions of V and Ti, which behave in a similar manner have been shown to reduce the extent of cracking during crush(2) although the precise mechanism is not clear. The AA6005A and AA6061 extrusions were also fully recrystallized but the grain size was coarser (~ 200µ for AA6061 and ~ 300µ for AA6005A) and more elongated than for the AA6008 as shown in Figures 10c, 10e and 10a respectively, due to the Mn and Cr additions made to these alloys. Although it would be possible to modify the composition and extrusion conditions for both alloys to produce a fully fibrous structure, the purpose of this study was to examine the effect of typical extruded microstructures on crush behavior. The AA6082 material exhibited a mixed grain structure with a coarse grain outer layer and a narrow fibrous core. The increased dispersoid concentration in this alloy due to the mandatory Mn addition is evident in Figure 10h. This composition is typical of a general purpose air quenchable AA6082 historically used in Europe for thin wall profiles. Finally the AA6082Cr variant exhibited a predominantly fibrous grain structure with a thin outer band of recrystallized grains. This form of AA6082 with a Cr addition is being increasingly used for automotive applications. Again the increase in dispersoid particle density compared to the standard AA6082 is evident when Figures 10h and 10j are compared. The extrusions were generally well solutionized during extrusion with limited undissolved Mg_2Si particles visible on the optical scale. The grain structures around the profile cross section were checked by macro-etching. These were uniform with the exception of the AA6082 variants where some grain coarsening at the weld line was evident as shown in Figure 11 for the AA6082Cr.

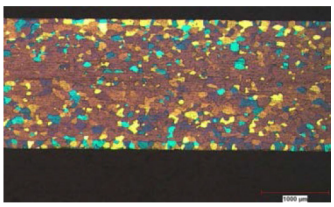

10a. AA6008

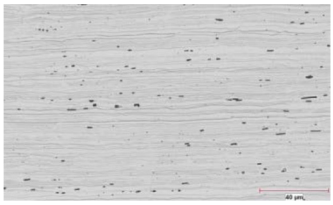

10b. A6008

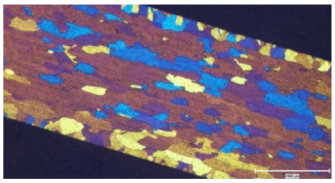

10c. AA6005A

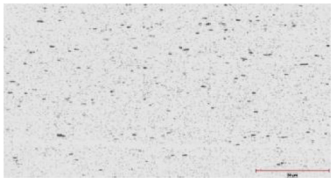

10d. AA6005A

Figure 10.

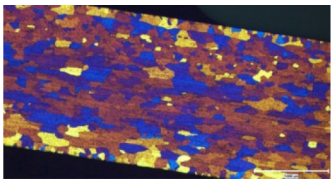

10e. AA6061

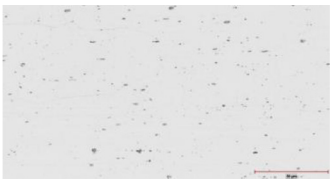

10f. AA6061

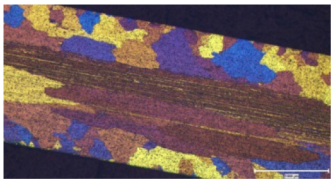

10g. AA6082

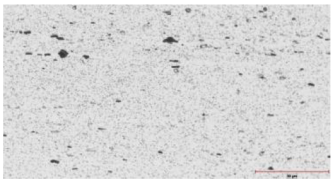

10h. AA6082

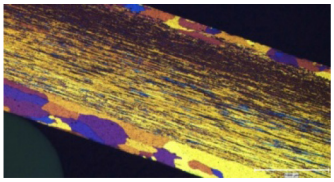

10i. AA6082Cr

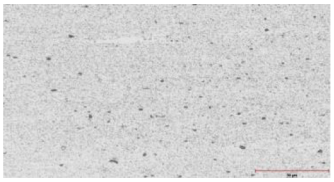

10j. AA6082Cr

Figure 10. (cont.) Longitudinal Microstructures of Medium Strength Alloys. (Barkers reagent- grain structure, 90s 0.5% HF - particle distribution)

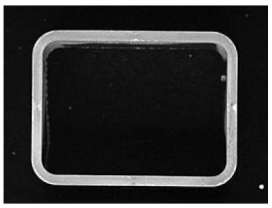

11a. Bulk Macrostructure

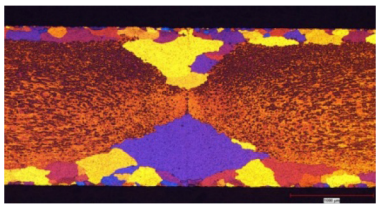

11b. Microstructure at weld line

Figure 11. Weld Line Microstructures for AA6082Cr

The maximum UTS values in MPa achieved for the five alloys for the peak aged condition increased in the following order (UTS values shown in parentheses):

AA6005A(305) < AA6008(313) < AA6061(322) < AA6082(325) < AA6082Cr(341).

Corresponding peak aged YS values again in the same order of increasing strength (with values in parentheses) were:

AA6005A(291) < AA6008(302) < AA6061(313) < AA6082(316) < AA6082Cr(322).

In all cases the peak UTS and peak YS corresponded to the same heat treatment condition which was 8 or 16 hrs/175°C except for AA6061 where peak strength was obtained with 3hrs/200°C. Therefore overall, the peak strength capability of the 5 alloys covered a range of ~30MPa YS and 35MPa UTS.

The linear relationship between MCF and UTS continued from the soft 6xxx into these medium strength alloys as shown in Figure 12. The results for all four soft 6XXX alloys are represented as the small black points. Although the medium strength alloys exhibited cracking grades ranging from 1 to 7 (internal and external transverse cracks and severe corner cracks) the fit is reasonable indicating this level of cracking

probably has minimal effect on energy absorption. The MCF value again did not correlate well with YS as shown in Figure 13 due to the effect of temper and the different response of underaged and overaged conditions. As was the case for the soft alloys in Figure 5, for the same YS value the under-aged tempers typically gave ~ 10% higher energy absorption due to their correspondingly higher UTS values.

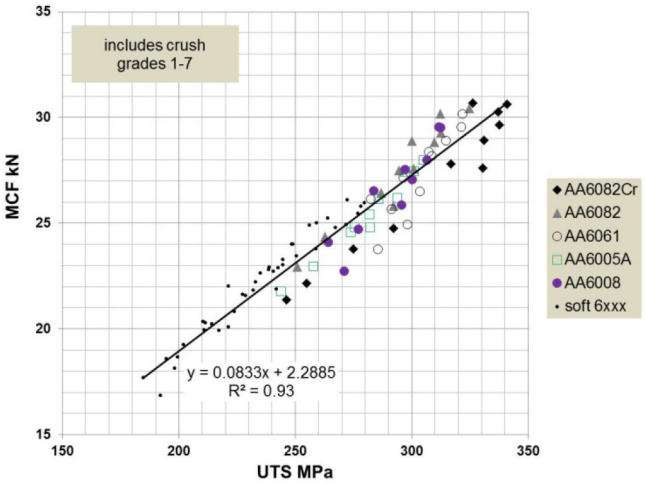

Figure 12. Mean Crush Force (MCF) vs. UTS All Alloys Tested.

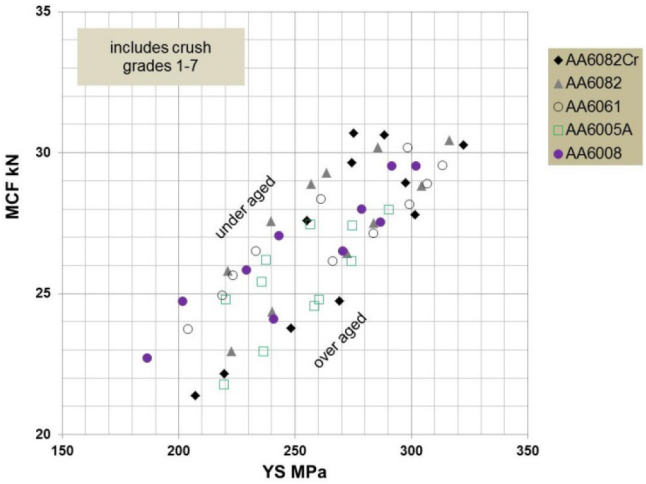

Figure 13. Mean Crush Force (MCF) vs. YS for Medium Strength Alloys (under-aged to over-aged clockwise)

The crush rating results for the medium strength alloys are summarized as a function of YS and UTS values in Figures 14 and 15 respectively. Although the crush grading is qualitative and non-linear some trends were apparent. From inspection of both figures it is clear that the AA6082 was inferior in terms of cracking tendency and had a grading 1 - 2 units higher than the other alloys for a given strength level. This can probably be attributed to the duplex fibrous and very coarse surface grain microstructure. Comparing the crush behavior of the other alloys, in the peak strength condition each 10-20MPa increase in YS or UTS was accompanied by a deterioration of 1 grade unit and no single alloy appeared to offer an advantage with the possible exception of AA6008. This alloy performed very well in these tests and although it exhibited grade 2 cracking in the peak aged condition it achieved the highest strength (287MPa YS, 300MPa UTS) corresponding to a zero cracking condition. When the AA6008 cracking tendency was assessed on a YS basis, as shown in Figure 14, over-ageing was clearly superior to under-ageing and the 2hrs/200°C treatment gave the highest YS for zero cracking condition. Interestingly, when the same results are compared on a UTS basis, as shown in Figure 15, the separation between over and under-aging is not apparent and the 16hrs/150°C treatment gave the highest UTS for a zero cracking condition. However, AA6008 still gave the highest UTS for a zero-crack condition. AA6061 exhibited similar behavior in terms of temper and an overaged treatment of 2.5hrs/215°C gave the best ranking/YS combination matching the peak aged AA6008. Again this trend was not apparent when the results were compared on a UTS basis. The other alloys did not exhibit a clear effect of under or overaging but this may have been lost in the limitations of the grading system. Overall, the AA6005A gave somewhat similar behavior to AA6008 but was generally 10-20MPa softer for the same crush grade. The AA6082Cr had the highest strength capability but this was achieved at the expense of the crush behavior. Compared to AA6061 it was capable of a 10-20MPa strength increase for the same crush grading but with continued softening by over or under-ageing its performance was still inferior to AA6008. Therefore AA6008 appears to offer some advantages in terms of crush behavior but it is not clear if this is due to the addition of V, the fine grain structure or the higher Mg/Si ratio or a combination of all of these factors.

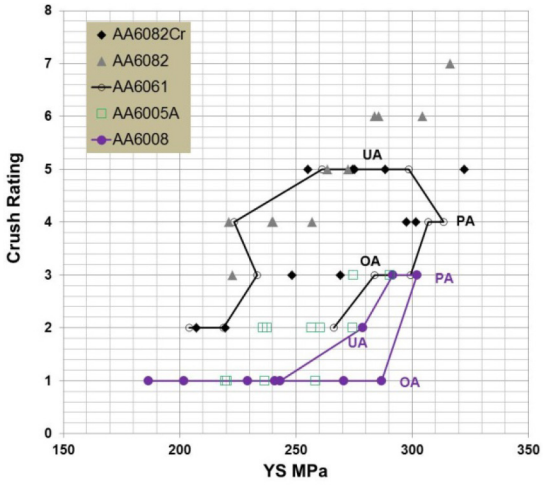

Figure 14. Crush grades vs. yield strength - medium strength alloys

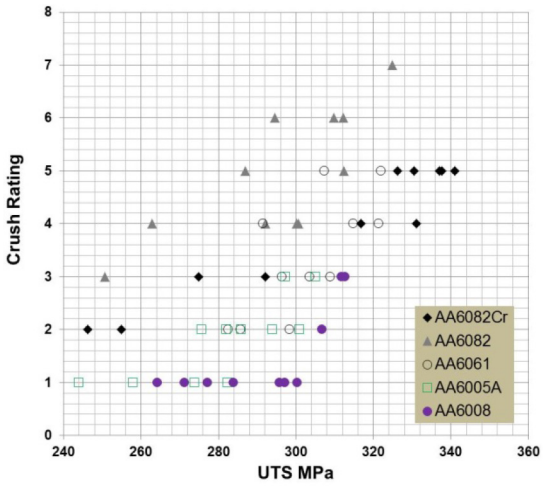

Figure 15. Crush grades vs. tensile strength - medium strength alloys

Figures 16 and 17 compare the crush behavior with the measures of ductility from the longitudinal tensile test. As was found with the soft 6xxx materials, tensile elongation (Fig 16) is a very poor predictor of

crush behavior. For a tensile elongation of ~ 8% the crush grade ranged from 1-7 and even an excellent tensile elongation of 20% gave crush rankings varying from 1-5. True fracture strain (ε_f) is a better indicator of crush performance as shown in Figure 17 with crush behavior generally improving as the ε_f value increased. The fine grained AA6008 exhibited a very clear cut off at 0.7 ε_f for the avoidance of cracking, corresponding to the value from the soft alloy results. Quite clearly the AA6082 condition that gave the poorest crush grades of 6 and 7 had the lowest ε_f values and the relationship was also reasonable for AA6005A and AA6061 although the ε_f cut-off for no cracks at 0.7 was not as evident. However, for the higher strength AA6082 alloys at intermediate crush grades there was considerable spread in the fracture strain for a given crush grading. For example AA6082Cr with a fracture strain of 1.0 only achieved a crush grade of 2. This effect is probably associated with the duplex coarse surface grain/fibrous core structures present in these materials. During the bending deformation associated with crush, the surface layers experience higher strains than the core. Although the fracture strain captures the deformation during necking it is probably less sensitive to coarse surface or duplex grain structures than bending or crush modes of deformation. On this basis the results suggest that with improved grain structure control the AA6082and AA6082Cr could perform significantly better in crush than the results of this study suggest.

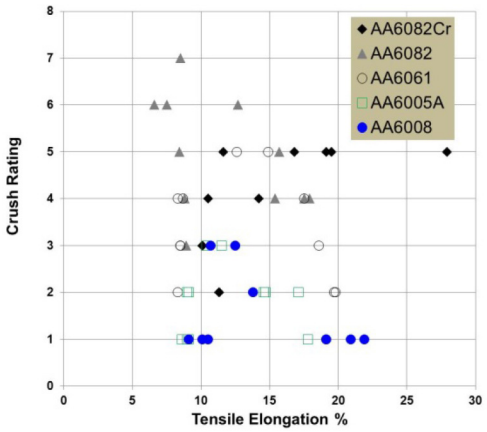

Figure 16. Crush grades vs. tensile elongation - medium strength alloys.

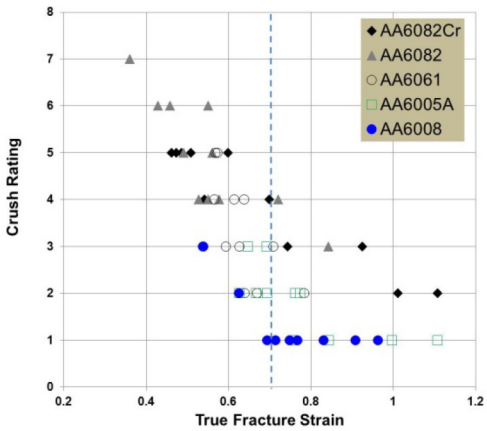

Figure 17. Crush grades vs. true fracture strain - medium strength alloys.

Discussion

The current study has compared the crush response of standard 6xxx commercial extrusion alloys with microstructures ranging from fully recrystallized fine grain to mixed unrecrystallized core/coarse grain recrystallized surface layer. Strength levels varied from 120 - 322 MPa YS and 180 - 341MPa UTS. Over this range of microstructures and properties there was a clear linear trend of increasing mean crush force, or energy absorption with increasing UTS value. If a crash structure is being designed to increase energy absorption then clearly it is important to specify and control the UTS value of the material. The linear trend for MCF and UTS was not significantly affected by the occurrence of cracking during crush at least up to grade 7 which did not include fragmentation. When energy absorption was compared on a YS basis there was a clear separation between under and overaged tempers with under-aging generally giving a 5-10% increase in MCF for the same YS. This is an interesting result as over-aging is often practiced commercially to increase material ductility. The situation is somewhat simpler when only peak aged properties are considered. As Figure 18 shows, the relationship between MCF and the peak aged yield strength is also linear. In this condition the difference between the YS and UTS is fairly consistent at 12-16MPa due to limited work hardening. Therefore if materials are used in the peak aged condition the YS is also a good predictor of energy absorption. If the material is deliberately softened for example by overaging, then UTS is the preferred measure of energy absorption.

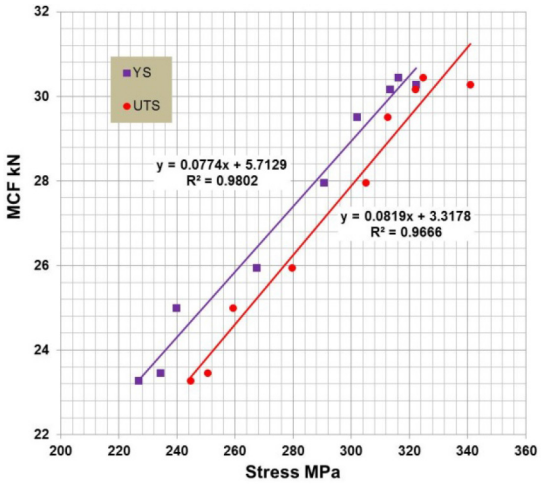

Figure 18. Effect of peak aged strength on mean crush force - all alloys.

The other aspect of crush performance of a material is clearly the onset and severity of cracking for a given geometry. The current study has reconfirmed for a wide range of microstructures and strength levels that tensile elongation is a very poor parameter for predicting cracking sensitivity and true fracture strain or reduction of area in a tensile test is much more useful. It is particularly accurate for soft fine grained 6xxx materials commonly used in crush systems today. It is still useful for stronger alloys but appears to be less sensitive to coarse surface grain structures which are more prone to surface cracking during crush than a tensile test.

Based on the knowledge that energy absorption as expressed by MCF is a linear function of the UTS and the onset of cracking can be predicted by the fracture strain, then the crush behavior of various alloy/temper/quench rate combinations tested can be summarized by plotting these two parameters as shown in Figure 19 for the soft

alloys. The most obvious feature of this diagram is that fracture strain decreases with increasing strength for all alloys, meaning that some increase in cracking tendency has to be anticipated if stronger materials are selected. However, the data also exhibits clear separation between water and air quenched extrusions with air quenching at the rates used in this study typically reducing the fracture strain achievable at a given strength level by ~ 0.3-0.4 such that several alloy/temper combinations resulted in a fracture strain below the critical value of 0.7 for this profile. This corresponded to increased severity of cracking in crush. The effect is due to the changes in grain boundary microstructure at lower quench rates, in particular the formation of coarse Mg_2Si precipitates that reduce the grain boundary strength. The range of quench rates investigated in the current study was extreme, but clearly this aspect of the extrusion process can have a significant effect on ductility in crash. For this reason, water quenching is typically specified for automotive extrusions, which presents challenges in terms of control of quench distortion to meet geometric requirements, and has led to widespread use of controllable spray quench systems.

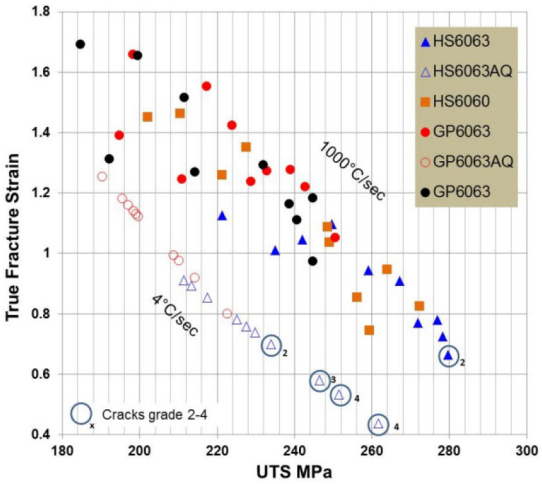

Figure 19. Fracture strain vs. tensile strength - soft alloys. (open symbols represent air quench, circles indicate cracking)

Figure 20 shows the relationship for all the alloy/temper combinations tested in the water quenched condition. Using the critical strain of 0.7 established for the current profile based on the crush rating - ε_f plots this allows the highest strength material to be selected meeting that criterion, which is AA6008 in a slightly softened temper. The diagram also allows inferior materials to be identified for example AA6082 typically gave the lowest ε_f values for a given UTS value. (Note that here we are referring to the specific alloy variant and microstructure produced in these tests and not AA6082 generically) As discussed earlier the fracture strain does not completely take into account the effect of coarse surface grain structures. Figure 21 shows how the coarse surface grain surface structures initiate cracking at the outer surface of the fold. These cracks are then arrested by the fibrous grain core. Although Figure 20 suggests that the AA6082Cr in a softened temper should not crack in crush at a UTS of ~ 315MPa, this material gave grade 4 cracking. However, this would suggest that with control of grain structure, perhaps through extrusion practice this type of material could be a higher strength solution.

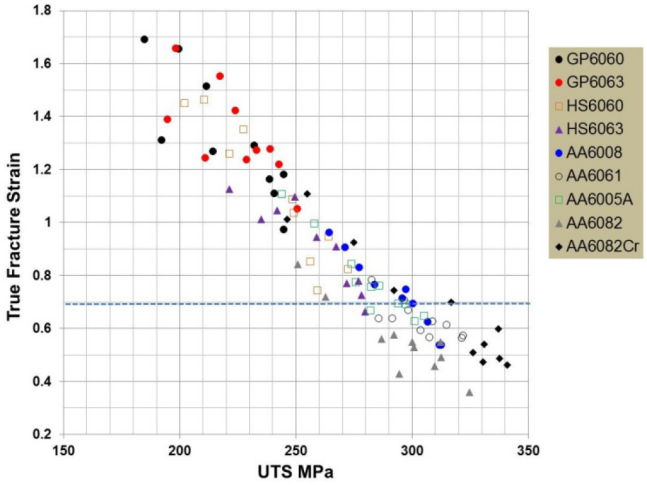

Figure 20. Fracture strain vs. tensile strength - all alloy/temper combinations - water quenched.

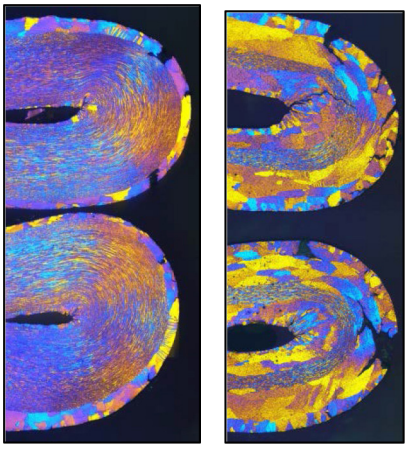

21a. AA6082Cr 21b. AA6082

Figure 21. Cross sections through crushed 6082 variants (Barkers Reagent)

It is interesting to examine the effect of temper on the data in Figure 20 more closely. Figure 22 presents ε_f - UTS values for selected alloys covering the overall strength range but separated by ageing temperature. The lower strength GP 6063 clearly shows some separation between over and underaged tempers with ageing at 200 and 215°C (squares and diamond symbols) offering superior fracture strain values for a given UTS. This trend was not evident in the crush tests as no cracking was encountered for this alloy but would suggest overageing can be beneficial for ductility during crush. This is in line with previous work[8] related to the effects of the shearable/non shearable transition on the interaction of ageing precipitates with slip and how this delays intergranular fracture. However, the effect is not apparent for the higher strength alloys with UTS values of >250MPa. When the same ε_f values are plotted against YS as shown in Figure 23, the benefits of overaging on fracture strain become apparent for all the alloys. This means it is probably possible for most alloys to sacrifice some strength by overageing to reduce cracking during crush if that is required. As described above this would be at the loss of some energy absorption. Figure 22 also suggests that peak aged alloys such as 6082Cr containing a fibrous grain structure and a high dispersoid content should be capable of increased strength and ductility. Furthermore, it may be possible to overage a stronger alloy, such as the AA6082Cr to provide superior ductility than say AA6008 for the same YS value. This was not borne out by the crush testing in

the current work but this may reflect the ability of the ε_f measurement to deal with surface grain size effects in these stronger alloys during crush. It does however indicate that with suitable microstructure control this may be one approach to improve crush behavior.

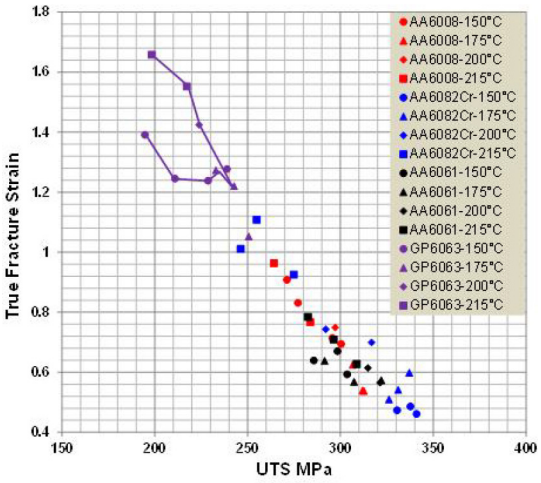

Figure 22. Fracture strain vs. tensile strength separated by ageing condition - GP6063, AA6008, AA6061 and AA6082Cr water quenched.

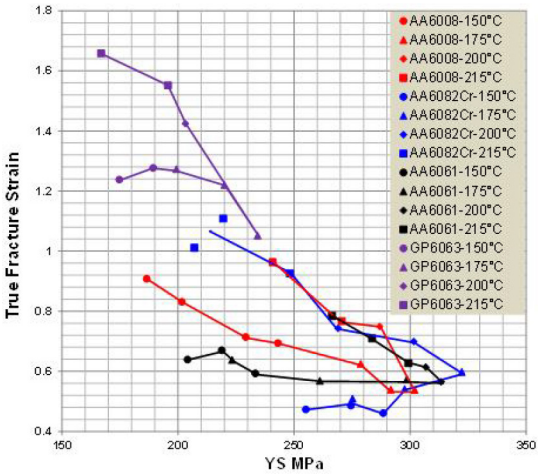

Figure 23. Fracture strain vs. yield strength separated by ageing condition - GP6063, AA6008, AA6061 and AA6082Cr water quenched.

Conclusions

- Alloy and temper selection for axial crush should consider energy absorption and cracking sensitivity. A design based on YS alone does not necessarily optimize the energy absorption aspect.
- The energy absorbed during crush, as measured by the mean crush force increases linearly with the tensile strength for a wide range of 6xxx alloys and tempers. For peak aged material yield strength also correlates well with energy absorption but for the same YS value, underaged tempers provide ~ 10% higher MCF than overaged.
- Tensile elongation is not a good predictor of cracking sensitivity during crush
- True fracture strain measured from a tensile test correlates well with the cracking tendency during crush although it appears to be less sensitive to through thickness microstructure variations such as coarse surface grain effects
- The increase in quench rate associated with the transition from air to water quenching significantly increases the fracture strain for a given strength level and is probably the most important extrusion parameter for control of ductility in crush.
- Overageing provides superior fracture strain values as compared to underaging for a given YS value and this was mirrored in some of the crush testing. However, this is accompanied by a reduction in MCF and energy absorption.
- Of the various alloys tested, water quenched AA6008 gave the highest strength associated with a zero cracking condition.

References

1. Tundal U., Reiso O., Skerjvold S. R., Kubiak A. D. “Al-Mg-Si Aluminium Alloy with Improved Properties” PCT Application - WO 2013/162374.
2. Royset J., Tundal U., Reiso O. and Furu T., “Al-Mg-Si Alloys with Improved Crush Properties”, Proceedings of the Ninth International Aluminum Extrusion Technology Seminar, 2008.
3. Rosefort M., Baumgart R., Matthies C., Koch H. “Influence of Microstructure on the Folding Behaviour of Crash Relevant Aluminum Extrusion Parts”. Light Metals pp 201, 2014
4. Baccouche. R., Miller C., Wagner D., Sherman A., Ward W. “Service Life Heat Exposure Effects and Aluminum Crash Property Relationships Under Static Axial Loading”. Proc. IMECE2006. Nov 5 - 10, 2006, Chicago USA. pp13
5. Rebuffet, O., Morère, B., Magnin, B., and Bompard, S., "Aluminium Extrusion Alloy Selection for Crashworthiness Energy Absorption and Failure," SAE Technical Paper 2002-01-2021, 2002, doi:10.4271/2002-01-2021.
6. Beland J-F., Parson N. C. “Evaluation of the Axial Crush Performance of Al-Mg-Si Extrusions”. Americas Conference on Aluminum Alloys. Aug 23-26. Toronto Canada. Paper 9121
7. Parson, N. C., Beland J.F., “Extrusions for Automotive Crash Applications”, Proceedings of the Eleventh International Extrusion Technology Seminar.
8. Poole W. J., Wang X., Lloyd D. J. and Embury J. D., “The shearable-non-shearable transition in Al-Mg-Si-Cu precipitation hardening alloys,” Phil Mag. Vol 85. Nos 26-27. 11-21 Sept 2005. 3113-3135.

Contact Information

nick.parson@riotinto.com

Acknowledgments

Sections of this paper are reprinted with permission from the Eleventh International Aluminum Extrusion Technology Seminar (ET’16) published by the Aluminum Extruders Council.

Definitions/Abbreviations

ε_f - True fracture strain

A_o - Initial tensile specimen cross section.

A_f - Cross section of final fracture

ISSN 0148-7191

http://papers.sae.org/2017-01-1272